

## Compression and strength of dense sand at high pressures and elevated temperatures

James Graham, Marolo Alfaro, and Gerald Ferris

**Abstract:** The paper examines the stress–strain behaviour of densely compacted sand tested at pressures up to 80 MPa in one-dimensional compression and 7.2 MPa confining pressure in triaxial tests. Tests were performed at temperatures up to 100 °C. The testing relates to a proposal by Atomic Energy of Canada Limited to fill containers of waste nuclear fuel with a crushed quartz sand to provide additional stiffness. No significant effects of temperature were encountered in either isotropic compression or triaxial shear.

*Key words:* sand, compression, shear strength, temperature, pressure.

**Résumé :** Cet article examine le comportement du sable compacté dans un état dense et testé à des pressions atteignant 80 MPa en compression 1D et 7,2 MPa de pression de confinement dans des essais triaxiaux. Les essais ont été réalisés à des températures atteignant 100 °C. Ces essais sont en rapport avec un projet de Énergie Atomique du Canada Ltée de remplir les contenants de déchets nucléaires avec du sable de quartz broyé pour fournir une rigidité additionnelle. Aucun effet significatif de la température n'a été observé dans la compression isotrope ou dans le cisaillement triaxial.

*Mots clés :* sable, compression, résistance au cisaillement, température, pression.

[Traduit par la Rédaction]

### Introduction

As part of their strategy for disposing of nuclear fuel waste deep in the Canadian Shield, Atomic Energy of Canada Limited (AECL) suggested using fine sand as a “filler” inside metal containers of fuel waste (AECL 1994). The AECL concept visualized containers surrounded by a seal (or “buffer”) of compacted sand–bentonite (Dixon et al. 2002). Under the likely groundwater pressures at the proposed depth of 500–1000 m in the granitic host rock and the swelling pressures exerted by the sand–bentonite, the container would deform as a “thin cylinder.” Deformations could lead to possible rupture of the container, especially near the ends, increased access of groundwater to the waste-form, and associated environmental hazards.

These performance requirements led to a proposal that the container should contain not only the waste-form but also a filler to increase its mechanical stiffness. The filler would

(i) support the waste-form; (ii) resist compression of the container under pressures from the groundwater and the buffer; (iii) be chemically neutral; and (iv) transfer heat effectively to the container, buffer, and surrounding rock. This project addressed the compressibility, strength, and deformability of the sand filler under high pressures and elevated temperatures.

Some initial studies examined bead soda glass “ballotini,” but these had unfavourable chemical interactions with the waste-form. Here we report results from 16–25 and 20–40 “frac” (for “fractured”) sand, a commercially available, crushed and washed, semiangular quartz sand (16–25, for example, refers to material that passes a 16 meshes per inch (1 in. = 25.4 mm) sieve and is retained on a 25 meshes per inch sieve). Physical properties of the sands are shown in Table 1.

The proposed application is strongly coupled. Heat flow from the waste-form into the rock produces temperature gradients. These in turn cause gradients in water content, density, and suction in the buffer and local changes in the strength and compressibility of the buffer (Dixon et al. 2002). Following emplacement, “wetting up” of the initially unsaturated buffer leads to transfer of a combination of swelling pressures and regional groundwater pressures to the container. It is anticipated that the resulting total pressures can reach 12–15 MPa at 1000 m depth. The pressures compress the fuel waste container and allow some expansion of the buffer. This in turn reduces pressure on the container.

Received 19 August 2003. Accepted 13 April 2004. Published on the NRC Research Press Web site at <http://cgj.nrc.ca> on 28 October 2004.

**J. Graham<sup>1</sup>** and **M. Alfaro.** Department of Civil Engineering, 342 Engineering Building, University of Manitoba, Winnipeg, MB R3T 5V6, Canada.

**G. Ferris.** BGC Engineering Inc., 840–7th Avenue SW, Calgary, AB T2P 3G2, Canada.

<sup>1</sup>Corresponding author (e-mail: [jgraham@cc.umanitoba.ca](mailto:jgraham@cc.umanitoba.ca)).

**Table 1.** Physical properties of the sands used in this study.

	16–25 frac sand	20–40 frac sand
Maximum specific volume, $V_{\max}$	1.707	1.712
Minimum specific volume, $V_{\min}$	1.416	0.432
Average specific weight of particles, $G_s$	2.64	2.65
Breakage potential, $B_p$	70.1	48.2
Maximum density, $\rho_{\max}$ (Mg/m <sup>3</sup> )	1.87	1.85
Minimum density, $\rho_{\min}$ (Mg/m <sup>3</sup> )	1.55	1.55
Average density index, $I_d$	0.82	0.75

**Note:** The breakage potential is the area on a gradation curve between the initial grading curve and a vertical line  $D = 0.074$  mm.

**Table 2.** Initial conditions and particle breakage in 1D compression tests on specimens T1809–T1813.

	T1809	T1810	T1811	T1812	T1813
Material (sieve size = no. of meshes per inch)	16–25	16–25	20–40	20–40	20–40
Initial specific volume, $V_o$	1.4711	1.4685	1.4730	1.5124	1.5221
Density index, $I_d$	0.811	0.820	0.854	0.713	0.678
Maximum pressure (MPa)	80.5	80.5	80.5	80.5	80.5
Pressure when breakage heard (MPa)	44	28	50	39	25
Breakage potential, $B_p$	70.1	70.1	48.2	48.2	48.2
Relative breakage, $B_r$	0.226	0.189	0.327	0.330	0.339

The processes change with time as the waste-form cools. Numerical modelling of the interactions requires deformation characteristics of densely compacted quartz sand at high pressures and elevated temperatures. Shearing sand specimens takes only a small amount of additional time. As a result, strength and compressibility tests were undertaken.

The proposed application required the sand filler to have both good compaction and good flow characteristics. Because of the size of spaces in the waste-form, a uniform particle size corresponding to a sieve size of (mostly) 20–40 meshes per inch was selected. This led to good flow characteristics but only average compaction.

The testing program consisted of a combination of one-dimensional (1D) compression tests at pressures up to 80 MPa and triaxial compression tests at confining pressures up to 7.2 MPa, with temperatures up to 100 °C. These pressures and temperatures are much higher than those normally used in geotechnical practice. Relative densities for the frac sand averaged 0.78 (Table 2). Again, this is outside the normal range of research testing, where concern is mostly about loose to medium-dense sands, for example in liquefaction problems and offshore construction (Sladen and Oswell 1989; Jefferies and Been 2000; but see McDowell et al. 2002).

Unlike clays, sands do not initially have unique normal compression lines (NCLs), which describe compression that is only partly recoverable (elastic–plastic) (Coop and Lee 1993). Jefferies and Been (2000) showed that sand specimens prepared to a variety of different initial densities will demonstrate different NCLs, each depending on the initial density or specific volume. The idea was first reported by Ishihara and Watanabe (1976) in laboratory experiments and then noted in the construction of artificial islands for petroleum exploration (Stewart et al. 1983). It is commonly (but not exclusively) understood that a unique compression line

is only achieved at high pressures after grain crushing becomes significant (for example, Miura et al. 1984; Coop 1990; Nakata et al. 2001; Klotz and Coop 2002). With the high pressures in the application proposed by the AECL, such crushing could become a concern.

## One-dimensional (1D) compression tests

### Test details

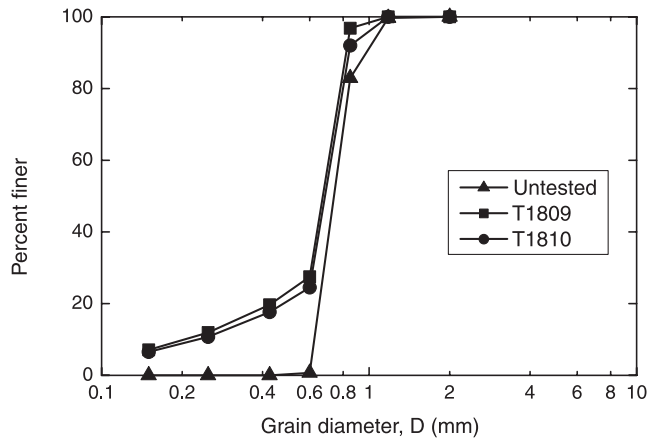
One-dimensional (1D) compression tests were used to reach axial pressures of 80 MPa, considerably higher than could be obtained in the available triaxial compression equipment. Similar programs were reported recently by Takei et al. (2001) and Nakata et al. (2001). The 1D compression cell was made of stainless steel with an outside diameter of 90 mm and an inside diameter of 64 mm (Ferris 2000). Observations in the 1D cell showed that pitting of the stainless steel started at an applied axial stress of about 40 MPa. Indentations on the surface of the AECL container could lead to reduced corrosion resistance.

Specimens were prepared in the cell through dry pluviation, with additional tamping and vibration to increase the density. Loading was performed using strain control, with stresses being measured at fixed increments of strain. After the tests were completed, sieve analyses were performed on the specimens to assess possible grain crushing.

### Results

Table 2 summarizes initial conditions, the maximum pressure reached in the 1D compression tests (80.5 MPa), the pressures when particle breakage was first heard (aurally, without instrumentation), and information about measurements of particle breakage. Sounds of particle breakage were first heard at pressures ranging from 28 to 50 MPa, with an average value of 37 MPa. Figure 1 shows typical particle-

**Fig. 1.** Results of sieve analysis before (untested) and after (specimens T1809 and T1810) testing.



size distribution curves before and after the 1D compression tests.

Observations of changes in particle-size distribution support the association of crushing sounds with particle breakage. Table 2 shows results in terms of breakage potential  $B_p$  and relative breakage  $B_r$  (Hardin 1985) (breakage potential is the area on a gradation curve between the initial grading curve and a vertical line at nominal particle diameter  $D = 0.074$  mm; relative breakage  $B_r$  is the ratio  $B_p/B_{p0}$ , where the total breakage  $B_t$  is the area between the initial and final grading curves at about  $D = 0.074$  mm). Even though the quartz particles were mechanically robust, testing pressures of 80.5 MPa caused significant breakage, which, naturally, was expressed in nonrecoverable deformations.

Figure 2 shows typical  $V - \log \sigma_a$  data from a 1D compression test at 27 °C (where  $V$  is the specific volume, and  $\sigma_a$  is the axial stress). Initially stiff behaviour is followed by subsequent more compressible, nonrecoverable behaviour. This test involved two relatively small unload–reload cycles that showed largely linear and nonhysteretic behaviour in semilogarithmic space. Final unloading back to a low pressure was also largely linear, and parallel to both the unload–reload cycles and the initial loading. The average unload–reload compression index from the 1D compression tests was  $\kappa = 0.0065$ , where  $\kappa = (V_i - V_j)/\ln(\sigma_i/\sigma_j)$ .

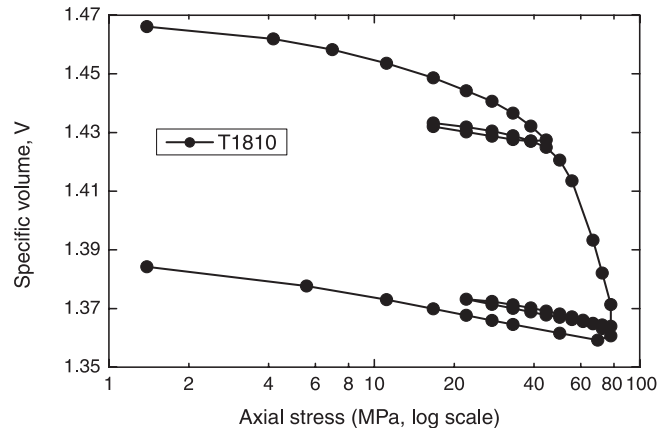
The behaviour became considerably more compressible when the vertical pressure exceeded about 30–40 MPa, the same range at which grain crushing became audible (Table 2). Many studies (for example, Miura et al. 1984; Pestana and Whittle 1995; Wood et al. 1994; Nakata et al. 2001; Klotz and Coop 2002) suggest that when grain crushing occurs, the behaviour approaches a single compression line in  $V - \ln \sigma_a$  plots. Results from this program (not shown for reasons of space) tend to support this assertion, with an average compression index  $\lambda_c = (V_m - V_n)/\ln(\sigma_n/\sigma_m) = 0.108$  in the region of grain crushing (Ferris 2000).

## Triaxial compression

### Test details

Triaxial testing was done in the high-temperature, high-pressure (HITEP) triaxial cell designed by Lingnau (1993). (Klotz and Coop 2002 and Hyodo et al. 2003 have reported

**Fig. 2.** Typical 1D compression results, including unload–reload cycles.



high-pressure triaxial tests on sand but only at room temperatures.) The HITEP cell features tie rods inside the sleeve, silicon oil cell fluid, pressure generation from compressed nitrogen, a resistance thermal device (RTD) for temperature measurement and control, an internal load cell, and internal axial and lateral displacement transducers mounted on the tie rods. The cell can operate safely at temperatures of 100 °C and cell pressures of 10 MPa (Graham et al. 2001).

Specimens were prepared in a way broadly similar to that for the 1D compression specimens, except that a split mould with an inner diameter of 63.5 mm was used and the length of the specimens was 127 mm. A standardized suction of 0.1 MPa was applied to allow the forming mould to be removed, the cell filled, and the confining pressure applied. Shearing was done with the drainage leads open to atmospheric pressure, so all measured stresses were effective stresses. Lubricated end platens were not used. Increments of isotropic confining pressure were first applied over a period of 1 day at room temperature, or 2 days if heated to 65 °C or 100 °C. Shearing to 12%–15% axial strain typically added one working day.

The maximum cell pressure was 10.4 MPa in the isotropic compression tests and 7.2 MPa in the triaxial compression tests. These values are much lower than the 30–40 MPa axial yield stress in the 1D tests. However, the addition of substantial deviator stresses in the triaxial compression tests was expected to lift the mean stress level towards the value in the 1D tests when crushing was first evident. The strain conditions in the two sets of tests were also different. It was felt that the lack of lateral confinement in the triaxial tests might lead to higher interparticle forces and earlier fracturing. Twenty-five triaxial tests were conducted on frac sand, nine at 27 °C (room temperature), nine at 65 °C, and seven at 100 °C. The average initial specific volume of the triaxial specimens was  $1.482 \pm 0.006$ , with an average density index  $I_d = 0.81$ . Shearing was continued to about 15% axial strain.

Isotropic compression testing up to a mean stress of 10.4 MPa did not produce measurable particle breakage when specimens were removed from the cell. In the triaxial compression tests, the combination of mean stress and deviator stress at peak failure at which breakage was first heard was approximately  $p_p = 8$  MPa and  $q_p = 10$  MPa, respectively (mean stress  $p = (\sigma_1 + 2\sigma_3)/3$  and deviator stress  $q =$

**Table 3.** Relationship between breakage and temperature in triaxial compression specimens.

	Temperature (°C)		
	27	65	100
Maximum mean stress at failure, $p_f$ (MPa)	12.0	12.3	12.0
Maximum deviator stress at failure, $q_f$ (MPa)	15.1	15.6	14.9
Total breakage, $B_t$	0.87	1.48	1.72

$\sigma_1 - \sigma_3$ , where  $\sigma_1$  and  $\sigma_3$  are the major and minor principal stresses, respectively). There was a small tendency for the amount of breakage to increase with an increase in temperature (Table 3).

**Results from isotropic compression tests**

Figures 3a and 3b show isotropic compression data at 27 °C and 100 °C, respectively. The deformation behaviour in semilogarithmic  $V - \ln(p)$  space at 27 °C was initially fairly straight, but then became curved up to about 10 MPa (Fig. 3a). It was apparently more linear at 100 °C, up to about 6 MPa (Fig. 3b). Only insignificant changes to particle-size distributions were seen in isotropic compression tests that were not followed by a shearing phase (Ferris 2000).

**Results from triaxial shear tests**

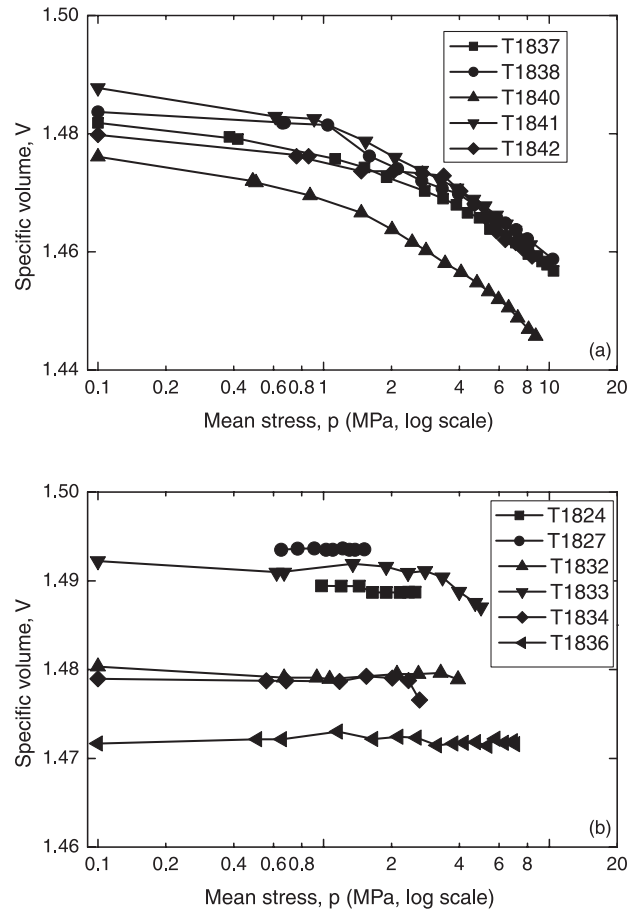
Figures 4a and 4b show typical graphs of deviator stress  $q = (\sigma_1 - \sigma_3)$  and volumetric strain  $\epsilon_v$ , respectively, versus shear strain  $\epsilon_s$  for tests performed at 100 °C with confining pressures ranging from 1.6 to 7.0 MPa. Volumetric strains were calculated from height and diameter changes using transducers reading directly on the specimens and assuming that the shape remained cylindrical. It is understood that this is only partly satisfactory in dense sands that dilate and generate strain concentrations in failure planes. The choice of simple instrumentation was in part influenced by the high confining pressures and temperatures used in the testing.

Even though the stress levels are high, the results show post-peak strain softening (Fig. 4a) and volumetric expansion (Fig. 4b) that are typical of dense sands. As usual, higher confining pressures tend to inhibit dilatancy. The strain softening and dilatancy seen in Fig. 4 probably reflect the angular to subangular shapes of the sand particles.

Figure 5 summarizes the peak strength data for all three temperatures. No clear differences were seen among strengths for different temperatures. The results have been separated, however, by whether particle crushing was observed after testing in particle-size distribution plots like those shown in Fig. 1. As is common, the peak strength envelope is slightly curved, with somewhat lower friction angles when high stress levels inhibit dilatancy.

Figure 6 shows “end-of-test” (EOT) values of  $q_{EOT}$  versus  $p_{EOT}$ . The data are again identified as being associated with specimens that exhibited no grain crushing and those that did. It seems reasonable to infer two linear sections of behaviour separated at  $p = 4.8$  MPa, one before crushing and the one with a flatter slope after crushing was observed in post-test measurements. The slopes of the two linear sections are  $\eta_{EOT} = 1.15$  and  $0.97$ , representing  $\phi'_{EOT}$  values of  $28.8^\circ$  and  $24.7^\circ$ , respectively, where  $\phi'_{EOT}$  is the end-of-test

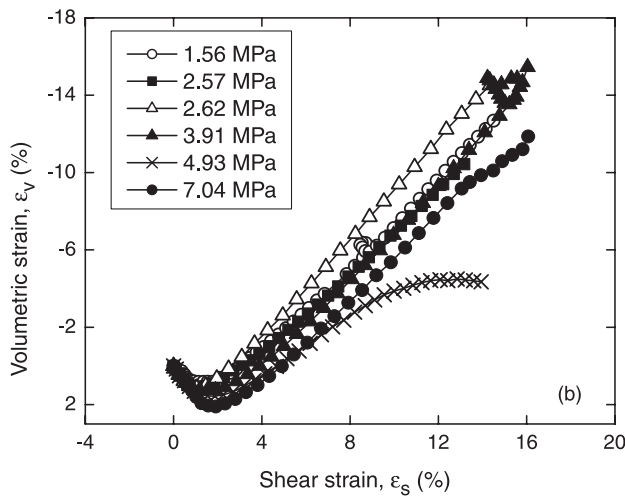
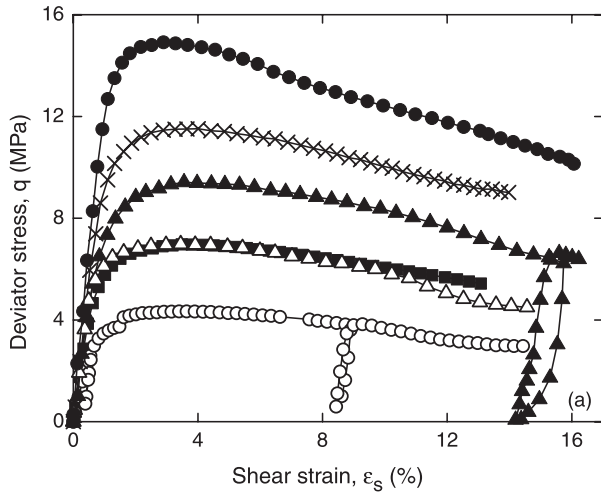
**Fig. 3.** Results from isotropic compression tests plotted as specific volume versus the logarithm of mean stress at (a) 27 °C and (b) 100 °C.



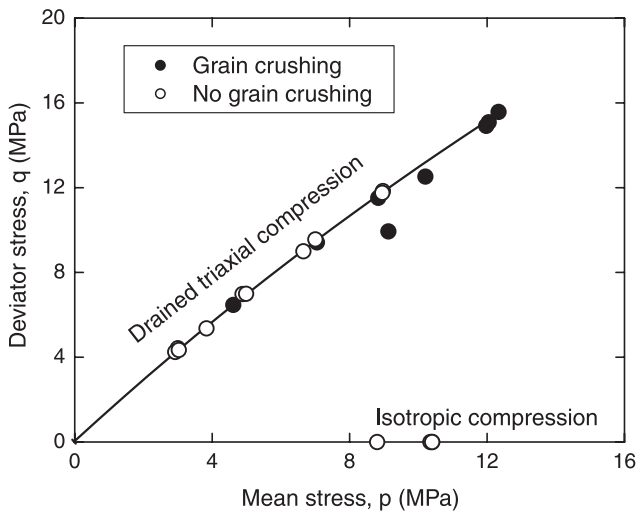
angle of shearing resistance. With increasing confining pressures, peak stress ratios  $\eta_p = [(\sigma_1 - \sigma_3)/(\sigma_1 + 2\sigma_3)]_p$  decrease towards end-of-test values, here taken as having constant (but different) values before crushing and after crushing (Fig. 7).

Figure 8 examines the relationship between end-of-test strengths (Fig. 6) and the shearing resistance at the “transition” deviator stress, defined as the deviator stress at which the volumetric strain rate  $\partial\epsilon_v/\partial\epsilon_s$  is zero in the early part of stress-strain graphs like those shown in Fig. 4. The transition data have again been modelled by a bilinear relationship for specimens that did not exhibit grain crushing and those that did. The slopes of the two sections of the transition envelope are  $\eta_t = 1.3$  and  $1.2$ , representing  $\phi'_t$  values of  $32.3^\circ$  and  $30.0^\circ$ , respectively. The change in slope occurred in this case at  $p = 6.4$  MPa. The bilinear envelope from the transi-

**Fig. 4.** Triaxial (compression) shear results for different confining stresses at 100 °C: (a) deviator stress  $q$  versus shear strain  $\epsilon_s$ ; (b) volume strain  $\epsilon_v$  versus shear strain  $\epsilon_s$ .



**Fig. 5.** Peak strength results for all temperatures (27 °C, 65 °C, and 100 °C) separated into specimens that exhibited grain crushing and those that did not.



**Fig. 6.** Bilinear end-of-test (EOT) strength envelope, indicating the presence of grain crushing during shear.

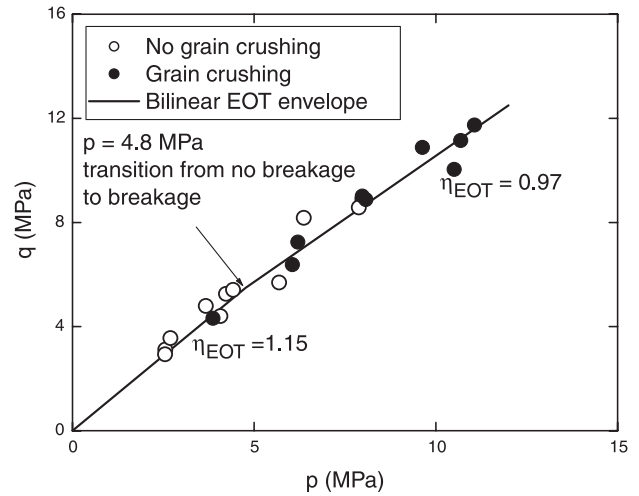


**Fig. 7.** Peak strength values of  $\eta_p = (q/p)_p$  plotted against confining pressure  $\sigma_r$ .

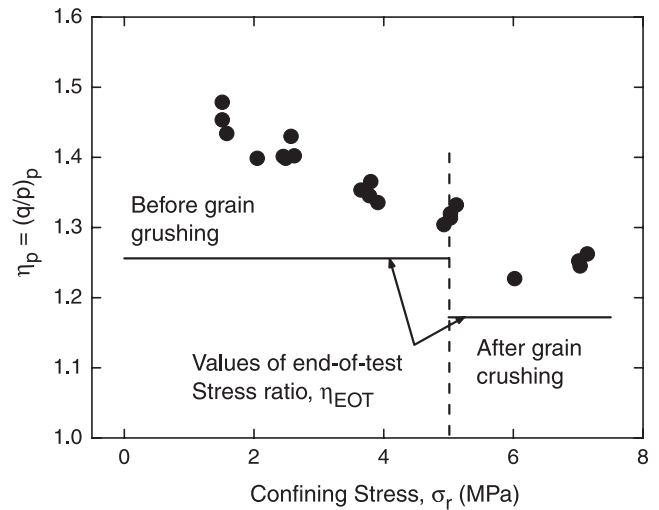


**Fig. 8.** End-of-test data plotted with transition data.

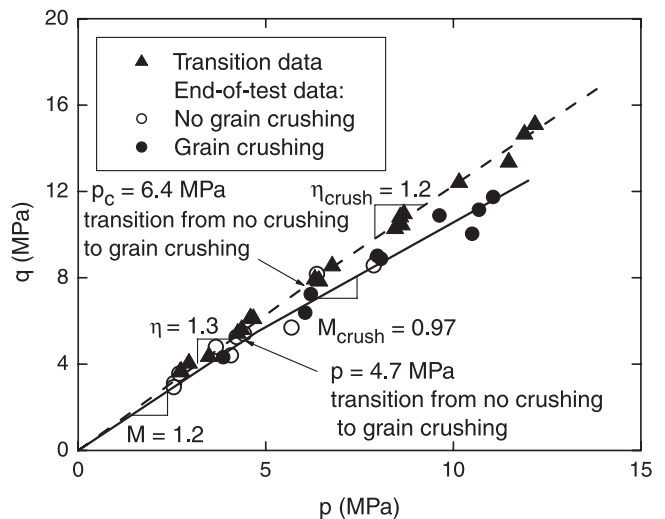
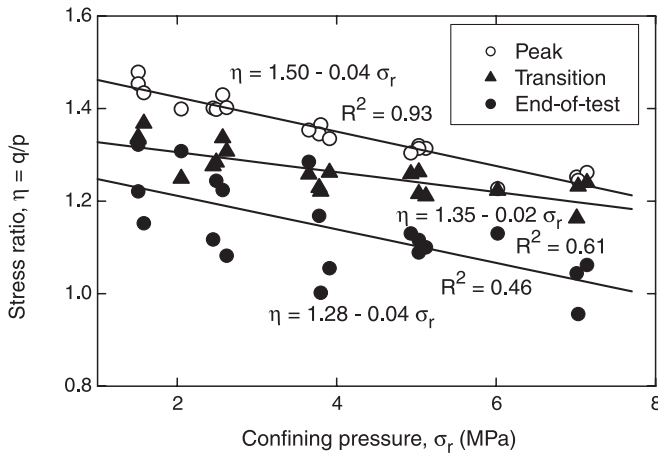


**Fig. 9.** Stress ratio  $\eta = q/p$  plotted against confining pressure  $\sigma_r$  for peak, transition, and end-of-test data.



tion data lies somewhat above the end-of-test envelope. This probably reflects lower specific volumes at the transition from compressive to expansive behaviour.

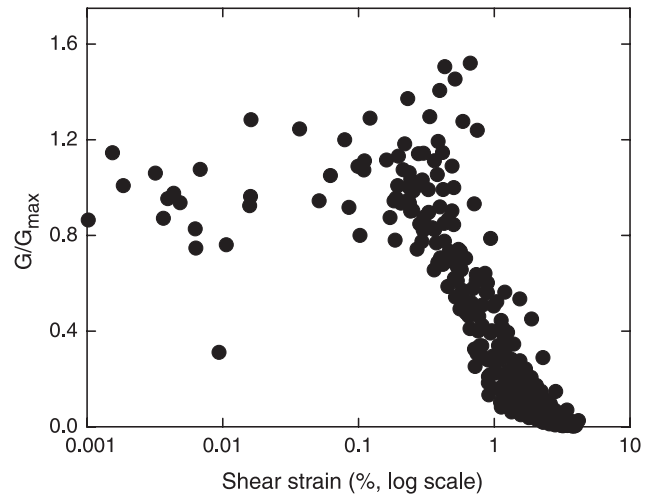
Figure 9 shows linear regression relationships among peak, transitional, and end-of-test stress ratios and confining pressure. These results are for all three testing temperatures and neglect the effect of crushing examined in Fig. 7. Decreasing values of  $\eta = q/p$  reflect how increasing confining pressures inhibit dilatancy and increase ductility. Figure 9 also shows the increasing differences between transitional data and end-of-test data as confining pressures increase. At the same time, differences between transitional data and peak strength data decrease. Here, the hoped-for agreement between end-of-test data and transitional data is not seen. This is thought to be because of the localized instrumentation in the specimens, strong development of failure surfaces in most specimens, and apparently strong dilatation right through to the end of testing (Fig. 4). The instrumentation does not permit confident identification of critical states in these tests.

**Shear modulus**

Like many laboratory and field programs, these tests show (Fig. 4) that prefailure shear stiffness  $G$  varies with shear strain  $\gamma$  and with pressure level (Iwasaki et al. 1978; Jardine et al. 1986). In general, such  $G$ - $\gamma$  relationships exhibit a substantially constant  $G_{max}$  at small strains, followed by an S-shaped curve in which the shear modulus  $G$  decreases to zero (by definition) at failure.

In the present study, the shear modulus was calculated incrementally in successive segments of  $q$  versus  $\epsilon_s$  data using a moving average over six data points. Figure 10 shows results from nine tests at 27 °C plotted as normalized shear modulus  $G/G_{max}$  versus shear strain  $\epsilon_s$ . It is recognized that the data show considerable scatter, but nevertheless some trends are clear. The initial range up to about  $\epsilon_s = 0.2\%$  corresponds to  $G_{max} = 63.8 + 11.6\sigma_c$ . That is, it increases with an increase in confining pressure  $\sigma_c$ . Peak failure, with  $G/G_{max} = 0$ , was reached at shear strains of between 2% and 4%. Summarizing the results from the three testing temperatures,  $G_{max}$  appears to decrease by perhaps 10% with temperature increasing from 27 °C to 100 °C. It is recognized

**Fig. 10.** Incrementally averaged values of normalized shear modulus  $G/G_{max}$  plotted against shear strain  $\epsilon_s$ .



that the scatter in the data is quite large and may be influenced by confining pressure.

**Concluding comments**

Tests have been done at temperatures up to 100 °C on high-density, air-dry specimens of frac sand at pressures up to 80 MPa in 1D compression and 10 MPa in triaxial compression. The results can be used to examine the suitability of frac sand as filler for stiffening thin-walled canisters for safe disposal of nuclear fuel waste.

Grain crushing was well developed and aurally evident at an axial stress of 30–40 MPa in 1D compression. In the triaxial tests it could be measured in particle-size analysis when the combined stress state was approximately 8 MPa mean stress and 10 MPa deviator stress.

For temperatures between 27 °C and 100 °C, strength envelopes did not seem to depend on temperature. End-of-test values of  $q, p$  states showed bilinear relationships separated into “noncrushing” and “grain-crushing” segments. There was some additional breakage of sand particles with higher temperature (Table 3), some increase in stiffness in isotropic loading, and perhaps a small reduction in the small-strain shear modulus  $G_{max}$ .

**Acknowledgements**

Financial support was provided by the Atomic Energy of Canada Limited, the CANDU Owners Group (COG), and the Natural Sciences and Engineering Research Council of Canada. Technical stimulus and advice were provided by Malcolm Gray, Brian Leetch, and Les Crosthwaite. Assistance with the testing and presentation was provided by Narong Piamsalee, Richie Armstrong, and Kendal Thiessen. The reviewers provided valuable comments that have been incorporated into the paper.

**References**

AECL. 1994. Environmental impact statement on the concept for disposal of Canada’s nuclear fuel waste. Atomic Energy of Can-

- ada Limited Report AECL-10711 and CANDU Owners Group Report COG-93-1.
- Coop, M.R. 1990. The mechanics of uncemented carbonate sands. *Géotechnique*, **40**: 607–626.
- Coop, M.R., and Lee, I.K. 1993. The behaviour of granular soils at elevated stresses. In *Predictive soil mechanics Edited by G.T. Houlsby and A.N. Schofield*. Thomas Telford, London, UK. pp. 186–199.
- Dixon, D., Chandler, N., Graham, J., and Gray, M.N. 2002. Two large-scale sealing tests conducted at Atomic Energy of Canada's underground research laboratory: the buffer-container experiment and the isothermal test. *Canadian Geotechnical Journal*, **39**: 503–518.
- Ferris, G.W. 2000. An elastic plastic approach: modelling deformation of dense sand. M.Sc. thesis, University of Manitoba, Winnipeg, Man.
- Graham, J., Tanaka, N., Crilly, T., and Alfaro, M. 2001. Modified Cam-Clay modelling of temperature effects in clays. *Canadian Geotechnical Journal*, **38**: 608–621.
- Hardin, B.O. 1985. Crushing of soil particles. *Journal of Geotechnical Engineering, ASCE*, **111**: 1177–1192.
- Hyodo, M., Yoshimoto, N., Nakata, Y., and Kuwajima, K. 2003. Undrained shear and particle crushing of sand under low and high confining stresses. In *Soil and Rock America: Proceedings of the 12th PanAmerican Conference on Soil Mechanics and Geotechnical Engineering*, Boston, Mass. 21–26 June 2003. Edited by P.J. Culligan, H.H. Einstein, and A.J. Whittle. Verlag Glückauf, Essen, Germany. pp. 577–581.
- Ishihara, K., and Watanabe, T. 1976. Sand liquefaction through volume decrease potential. *Soils and Foundations*, **16**: 61–70.
- Iwasaki, T., Tatsouka, F., and Takagi, Y. 1978. Shear moduli of sands under cyclic torsional shear loading. *Soils and Foundations*, **18**: 39–56.
- Jardine, R.J., Potts, D.M., Fourie, A.B., and Burland, J.B. 1986. Studies of the influence of non-linear stress-strain characteristics in soil-structure interaction. *Géotechnique*, **36**: 377–396.
- Jefferies, M., and Been, K. 2000. Implications for critical state theory from isotropic compression of sand. *Géotechnique*, **50**: 419–429.
- Klotz, E.U., and Coop, M.R. 2002. On the identification of critical state lines for sands. *Geotechnical Testing Journal*, **25**: 1–14.
- Lingnau, B.E. 1993. Consolidated undrained-triaxial behaviour of a sand-bentonite mixture at elevated temperature. Ph.D. thesis, University of Manitoba, Winnipeg, Man.
- McDowell, G.R., Nakata, Y., and Hyodo, M. 2002. On the plastic hardening of sand. *Géotechnique*, **52**: 349–358.
- Miura, N., Murata, H., and Yasufuku, N. 1984. Stress-strain characteristics of sand in a particle crushing region. *Soils and Foundations*, **24**: 77–89.
- Nakata, Y., Hyodo, M., Hyde, A.F.L., Kato, Y., and Murata, H. 2001. Microscopic particle crushing of sand subjected to high pressure one-dimensional compression. *Soils and Foundations*, **41**: 69–82.
- Pestana, J.M., and Whittle, A.J. 1995. Compression model for cohesionless soils. *Géotechnique*, **45**: 611–631.
- Sladen, J.A., and Oswell, J.M. 1989. The behaviour of very loose sand in the triaxial compression test. *Canadian Geotechnical Journal*, **26**: 103–113.
- Stewart, H.R., Jefferies, M.G., and Goldby, H. 1983. Berm construction for Gulf Canada Mobile Arctic Caisson. In *Proceedings of the 15th Annual Offshore Technology Conference*, Houston, Tex. 2–4 May 1983. Paper OTC 4552.
- Takei, M., Kusakabe, O., and Hayashi, T. 2001. Time-dependent behavior of crushable materials in one-dimensional compression tests. *Soils and Foundations*, **41**: 97–121.
- Wood, D.M., Belkheir, K., and Liu, D.F. 1994. Strain softening and state parameter for sand modelling. *Géotechnique*, **44**: 335–339.

### List of symbols

$B_p$	breakage potential
$B_r$	relative breakage
$B_t$	total breakage
$D$	nominal particle diameter
$G, G_s$	shear modulus
$G_s$	average specific weight of soil particles
$I_d$	density index
$M$	slope of strength envelope in $q$ vs. $p$ space
$p$	mean stress = $(\sigma_1 + 2\sigma_3)/3$
$q$	deviator stress = $(\sigma_1 - \sigma_3)$
$R^2$	correlation coefficient
$V$	specific volume = $(1 + e)$ , where $e$ is the voids ratio
$V_o$	initial specific volume
$\phi'$	angle of shearing resistance, effective stresses
$\gamma$	shear strain
$\eta$	stress ratio $q/p$
$\kappa$	slope of unload-reload line in $V - \ln \sigma_a$ plots
$\lambda_c$	slope of grain-crushing line in $V - \ln \sigma_a$ plot
$\epsilon_s$	shear strain
$\epsilon_v$	volumetric strain
$\rho$	dry density
$\sigma_1, \sigma_3$	major and minor principal stresses
$\sigma_a$	axial stress
$\sigma_r$	confining stress

### Subscripts

a, c, crush, EOT,	axial, confining, crushing, end-of-test, maxi-
max, min	imum, minimum
$i, j; m, n$	successive data points in unload-reload and particle-crushing stress ranges, respectively
p, t	peak, transitional